

Itinerant–electron magnetism: the importance of many-body correlations

Markus Holzmann

*Univ. Grenoble Alpes, CNRS, LPMMC, 38000 Grenoble, France and
Institut Laue Langevin, BP 156, F-38042 Grenoble Cedex 9, France*

Saverio Moroni

*CNR-IOM DEMOCRITOS, Istituto Officina dei Materiali,
and SISSA Scuola Internazionale Superiore di Studi Avanzati, Via Bonomea 265, I-34136 Trieste, Italy*

Do electrons become ferromagnetic just because of their repulsive Coulomb interaction? Our calculations on the three-dimensional electron gas imply that itinerant ferromagnetism of delocalized electrons without lattice and band structure, the most basic model considered by Stoner, is suppressed due to many-body correlations as speculated already by Wigner, and a possible ferromagnetic transition lowering the density is precluded by the formation of the Wigner crystal.

In 1929, Felix Bloch addressed the possibility of itinerant ferromagnetism¹ where the same electrons forming the conducting state give also rise to ferromagnetism. Considering the free homogeneous electron gas (jellium) as a minimal model to describe electrons in a metal, he concluded that the exchange energy may lead to a ferromagnetic state at densities slightly below those occurring in alkali metals. Considering correlation between positions of electrons with antiparallel spin, Wigner^{2,3} approximately calculated the correlation energy – the gain of energy compared to the Hartree-Fock approximation – and pointed out the possibility of crystalline order at low densities. In the same paper², he also anticipated that the magnitude of the correlation energy is important for questions of para– and ferromagnetism modifying Bloch’s theory on itinerant magnetism. Later, Stoner⁴ predicted the occurrence of a continuous transition between zero and full magnetization at zero temperature introducing a repulsive energy term between opposite spin electrons to phenomenologically account for correlation effects. The threshold of the ratio between this repulsive interaction constant and the Fermi energy, is now commonly known as Stoner criterion.

The question whether pure Coulomb interactions between electrons can drive a magnetization transition without accompanying structural changes has a long and controversial history, starting from Bloch’s prediction¹. Based on the Hartree-Fock approximation, he considered the possibility of a first order (discontinuous) transition to a fully polarized, ferromagnetic electron liquid for electronic densities, n , slightly lower than those of alkaline metals, $r_s \equiv a/a_B > 5.45$, where a_B is the Bohr radius and $a = (4\pi n/3)^{-1/3}$ is the mean electron distance. The first variational Monte Carlo (VMC) calculations⁵ taking into account electron correlations without relying on perturbative high or low density expansions indicated a totally polarized quantum fluid for $r_s > 26(5)$ before the occurrence of a Wigner crystal at $r_s = 67(5)$. More accurate calculations based on fixed-node diffusion Monte Carlo (DMC) and transient estimates releasing the nodal constraint subsequently shifted the ferromagnetic liquid to lower densities^{6,7}, $75(5) < r_s < 100(20)$. Later

calculations⁸ predicted a partial polarization of up to 50% in the range $20 \lesssim r_s \lesssim 100$. Two decades later, new calculations⁹ with larger system sizes observed a continuous transition from the paramagnetic to the ferromagnetic fluid around $r_s = 20(5)$ reaching full polarization around $r_s = 40(5)$ before freezing at $r_s = 65(10)$. The most recent quantum Monte Carlo (QMC) calculations¹⁰, reducing systematic errors of the thermodynamic limit extrapolation and of the fixed-node bias, again support Stoner’s picture of a continuous magnetic transition, but with an onset of partial spin polarization at $r_s = 50(2)$ and completion of full polarization at $r_s \approx 100$, just before Wigner crystallization which is estimated to occur at $r_s = 106(1)$ in Ref. 11.

Physical realization of such low density electron liquids at low temperatures is extremely challenging, and experimental findings¹² are controversial due to finite temperature and band structure effects^{13,14}. Recent experimental efforts have been devoted to realize Stoner’s model within ultracold atomic gases^{15,16}, where the interaction between two fermions is essentially described by momentum and energy independent s-wave scattering. However, there, the strong repulsive s-wave interaction is intrinsically connected with a short range interparticle bound state leading to molecule formation. Although local spin-correlations have been observed, the interpretation of the experimental observations is not straightforward.

In this paper, we show that Stoner’s instability is precluded by the transition to the Wigner crystal and argue that itinerant magnetism is quite generally suppressed by correlation effects in the ground state of homogeneous quantum fluids with spin-independent repulsive interactions. Specifically, we present new results for jellium in three dimensions based on a sequence of wave functions featuring iterative backflow transformations^{17,18}, within the variational and the more accurate fixed-phase diffusion Monte Carlo methods^{19,20}. Zero-variance extrapolation¹⁷ of the ground state energies at finite system size allows us to reliably control the remaining, systematic bias of the fixed-phase DMC calculations. Finite size corrections due to single-particle shell effects²¹ and two-body terms^{22–24} are applied for thermodynamic

limit extrapolation. Improved accuracy proves crucial, as our calculations show that many-body correlations of the ground state wave function favor the unpolarized phase of the electron liquid compared to partial or fully polarized states and eventually prevent itinerant magnetism in jellium at any densities above crystallization. We also update the density of the transition to the Wigner crystal to a slightly lower value, $r_s = 113(2)$.

Methodological and computational improvements of the accuracy of QMC calculations thus seem to parallel the historical developments on the two dimensional electron gas. The first QMC results^{5,25} indicated an intermediate region with a fully polarized liquid ground state, shrinking, subsequently, to a weakly first-order polarization transition occurring just before Wigner crystallization^{26,27}, and, finally, disappearing completely²⁸ following improvements to the fixed node bias and finite size methodology.

Taking further into account the absence of a polarized phase in ^3He , a strongly correlated Fermi liquid with an effective dominant hard-core interaction, we arrive at the quite general conclusion that pure correlation effects in homogeneous quantum liquids tend to suppress itinerant magnetization, in contrast to common argumentations based on Stoner's model. In these systems, crystallization, the spontaneous breaking of translational symmetry, seems to win the competition against spontaneous magnetization.

In the following, we describe the details of our numerical methods to determine the low-density ground state phase diagram of jellium – non-relativistic electrons interacting via Coulomb's potential with each other and with a homogeneous positive background to guarantee charge neutrality^{29,30}. The ground state energy per electron of the model at three values of the electronic density, n , corresponding to $r_s = 70, 100$, and 120 , and six different spin polarizations $\zeta = 0.0, 0.18, 0.42, 0.61, 0.79$, and 1.0 , is addressed by variational and diffusion Monte Carlo simulations¹⁹ of a finite system containing $N = 66$ electrons imposing periodic boundary conditions for the particles' positions; the long-range Coulomb potential is evaluated by standard splitting into real and reciprocal space contributions^{31,32}.

In the DMC runs³³, the number of walkers is 1280 and the time step is 15, 20, and 30 Ry^{-1} for $r_s = 70, 100$, and 120 , respectively. The estimated time step error is 10^{-7} Ry or less, which is about the size of the statistical error on our final results (the zero-variance extrapolation of the DMC energy, see below). The population control bias is even smaller, of the order of 10^{-8} Ry.

The accuracy of the ground state energy of a finite system is limited by the underlying many-body trial wave function Ψ used for calculating expectation values in VMC¹⁹ and for imposing the phase in DMC²⁰, respectively. In order to remove such a bias, we consider a series of trial wave functions of increasing quality, starting from the standard Jastrow-Slater and backflow forms (SJ and BF0)¹⁰, and adding up to four iterative backflow

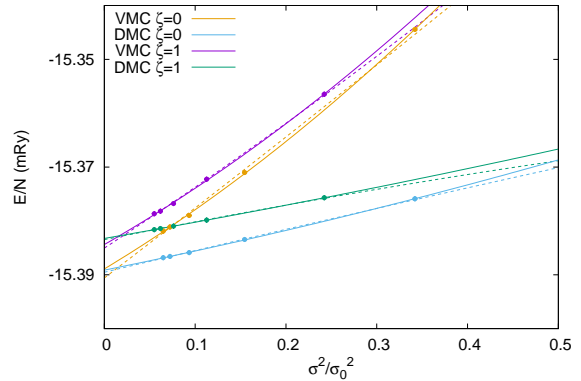


FIG. 1. Extrapolation of the energy to zero variance for $r_s = 100$ at polarizations $\zeta=0$ and 1 . The data are calculated with VMC and DMC using SJ, BF0, ..., BF4 wave functions in order of decreasing energy. The reference value σ_0^2 is the variance of the local energy at $\zeta=0$ with the SJ wave function. The curves are quadratic fits; for each set of data points (VMC and DMC for $\zeta=0$ and 1) there are two curves, one of which (solid line) excludes the SJ energy from the fit.

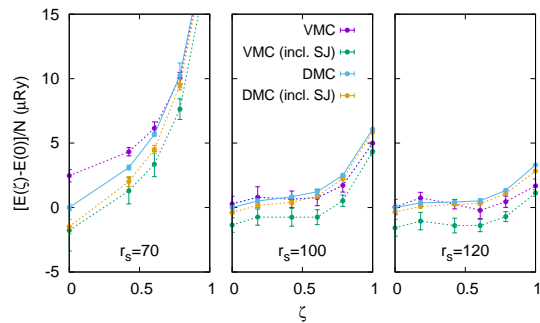


FIG. 2. The polarization energy $E(\zeta) - E(0)$ obtained from zero-variance extrapolations of the VMC and DMC energies, including or excluding the SJ result. The common reference energy $E(0)$ is the zero-variance extrapolation of the DMC energy without the SJ data.

transformations (BF1, ..., BF4)¹⁷.

Specifically, the Jastrow-Slater wave function $\text{SJ}(\mathbf{R})$ explicitly depends on the coordinates \mathbf{R} of all the particles through the two-body pseudopotential u_0 in the Jastrow factor $\exp(-U_0(\mathbf{R}))$, and through plane-wave orbitals in the Slater determinant $D(\mathbf{R})$. We then recursively build sets of transformed coordinates $\mathbf{Q}_0, \dots, \mathbf{Q}_k$, where \mathbf{Q}_i depends on \mathbf{Q}_{i-1} through the i -th backflow pseudopotential η_i , with $\mathbf{Q}_{-1} \equiv \mathbf{R}$. The k -th iterative

backflow wave function is

$$\text{BF}k(\mathbf{R}) = \exp(-U_0(\mathbf{Q}_{-1}) - \dots - U_k(\mathbf{Q}_{k-1}))D(\mathbf{Q}_k). \quad (1)$$

For the backflow wave functions we include both two- and three-body pseudopotentials u_0 and ξ_0 in $\exp(-U_0)$, and only two-body pseudopotentials u_i in $\exp(-U_i)$ for $i = 1, \dots, k$. The plane-wave orbitals in the Slater determinant are evaluated at the last set of transformed coordinates, \mathbf{Q}_k .

The two-body pseudopotential u_0 is initially of the the RPA form⁵ with an explicit long-range part in Fourier space spanning the first 20 shells of reciprocal vectors, and the real-space part represented by locally piecewise-quintic Hermite interpolants (LPQHI) with 8 degrees of freedom which are subsequently treated as optimization parameters. The three-body pseudopotential (ξ_0), the backflow pseudopotentials (η_i with $i = 0, \dots, k$), and the two-body pseudopotentials in the transformed coordinates (u_i with $i = 1, \dots, k$) are all expressed as LPQHI with 6 degrees of freedom each, with the exception of η_0 which is augmented with 5 shells of Fourier components. The LPQHI coefficients of all the pseudopotentials, as well as the Fourier components of η_0 , are optimized independently for each wave function in the hierarchy.

The energy E computed for $r_s = 100$ in VMC and DMC simulations using all the above wave functions is plotted in Fig. 1 against the corresponding VMC variance $\sigma^2 = \langle \Psi | (H - \langle H \rangle) | \Psi \rangle^2 | \Psi \rangle$. The exact ground-state energy, which has zero variance, can be reliably estimated by extrapolation¹⁷, given the smoothness of the data over a significant range extending to very low values of σ^2 . We assume a quadratic dependence of E on σ^2 . Since the range of validity of such a dependence is not known, we perform the extrapolation with and without the highest energies and variances, obtained with the SJ wave function. The result does not change significantly if we include the SJ result and/or switch between VMC and DMC data for the extrapolation. In particular, Figure 2 shows that the polarization energy is only marginally influenced by the choice of the data set.

Twist-averaged boundary conditions^{21,33} are used to reduce shell effects of the finite simulation cell and afford thermodynamic limit extrapolation without resorting to large simulation cells. Residual single particle shell effects due to the discrete twist grid and to reduced-symmetry open-shell fillings for finite polarizations with $N = 66$, ΔT_0 , are estimated from the non-interacting electron gas. Two-particle finite size corrections for the potential and kinetic energy, ΔFSE , are addressed by interpolation of the long-range part of the static structure factor and by the analytical long-range expressions for the two-body and backflow pseudopotentials u_0 and η_0 of the wavefunction^{23,34,35}. In contrast to the high density limit^{36,37}, where residual size effects in the kinetic energy introduce quasi-random fluctuations in the extrapolation, these effects are suppressed in the large r_s region addressed here (see Supplementary Material³³). Furthermore, at low densities, the corrections ΔFSE

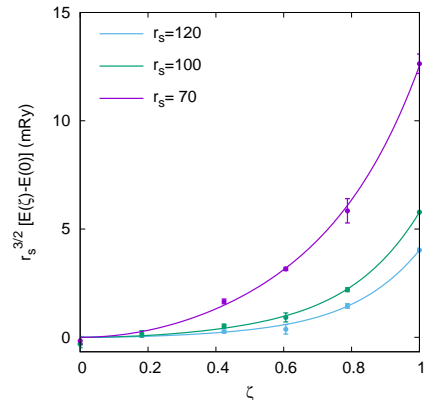


FIG. 3. The polarization energy $E(\zeta) - E(0)$ obtained from zero-variance extrapolations of the DMC energies without the SJ result. The lines are polynomial fits with terms of order 0, 2 and 6. Alternative functional forms and ensuing confidence levels for our conclusions are discussed in the Supplemental Material³³.

are largely dominated by the zero-point energy of the plasmon²². Whereas the single particle size corrections depend on the spin polarization, the long-range structure factor does not reveal any systematic dependence on ζ within the statistical error of the present simulations. Therefore, we average the structure factor over spin-polarizations in the calculation of ΔFSE , so that the final polarization energy is not affected by statistical fluctuations in the estimates of ΔFSE . Only the absolute value of the estimated ground state energy, used below to locate the Wigner crystallization, is then susceptible to the details of the calculation of ΔFSE .

The results for the energies and the variances obtained with different trial wave functions, the zero-variance extrapolations, and the finite-size corrections are collected in the Supplemental Material³³. Note that the variance extrapolation is done on the energies of the finite-size system, and size corrections (for the polarization energy and the Wigner crystallization) are applied afterwards, using the value of ΔFSE obtained at the highest wave function level.

The final polarization energy of jellium at low densities, our main result, is shown in Fig. 3 for $r_s = 70, 100$ and 120. It is obtained from the zero-variance extrapolation of the DMC energy, excluding the SJ result. This choice gives the smoothest polarization energy, as well as the lowest χ^2 in the fit to the energy vs. variance data, but it is otherwise uninfluential for the outcome that $E(\zeta)$ is higher than $E(0)$ for all the densities considered, and therefore a partially or fully polarized state is never stable. Confidence levels for our conclusion are given in the Supplemental Material³³.

The zero-variance extrapolation of the DMC energy, corrected for finite-size effects, is compared in Fig. 4

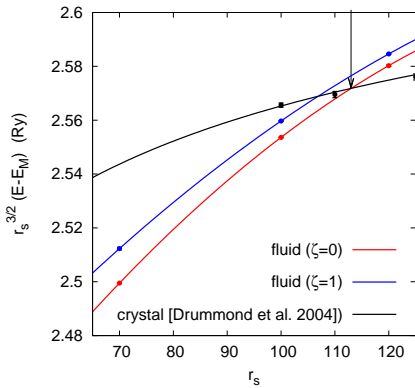


FIG. 4. DMC energy as a function of r_s for the paramagnetic and the ferromagnetic fluid and for the Wigner crystal. $E_M = -1.79186/r_s$ Ry is the Madelung energy of the bcc lattice¹¹. The lines are quadratic interpolations for the fluid phases, and a fit of the form¹¹ $a + b/\sqrt{r_s}$ for the Wigner crystal. The arrow at $r_s = 113$ locates the crystallization point.

with the fixed-node DMC energy¹⁹ of the Wigner crystal of Ref.¹¹ as a function of r_s . For the crystal phase, finite-size effects are assessed using large simulation cells with up to 512 electrons¹¹. This procedure differs from that used in the present work for the liquid phase, but it should be equally reliable. The fixed-node DMC bias¹⁹ for the crystal phase is negligible: it is bounded by (and presumably much smaller than) the difference between the fixed-node energy and the exact bosonic ground-state energy, which we find to be of the order of the statistical error on the crystal data of Fig. 4. The critical value for the Wigner crystallization is shifted to $r_s = 113(2)$, where the uncertainty includes both the statistical error of the simulation data and a conservative estimate of the residual bias in the size corrections³³.

In this paper, we have presented accurate quantum Monte Carlo calculations addressing the possibility of a

magnetically polarized fluid in the ground state phase diagram of the homogeneous electron gas. We have shown that iterated backflow wave functions^{17,18} provide highly accurate results for the energy and very low values of its variance, such that a zero variance extrapolation provides fairly unbiased results for the polarization energy. Our calculations clearly demonstrate that the simple mean-field picture based on Stoner's model is not sufficient to explain itinerant ferromagnetism as the partially or fully polarized fluid state is unstable versus Wigner crystallization.

Therefore, in addition to repulsive interparticle interactions, band structure effects must play an essential role for the occurrence of itinerant ferromagnetism in real materials.

Similar results have been found for liquid ³He in two^{17,38} and three dimensions^{18,39}, the two dimensional electron gas²⁸, and two dimensional quantum gases with repulsive dipolar interaction⁴⁰, where accurate, quantitative treatment of correlation effects have always stabilized the spin-unpolarized phase.

From a more general point of view, Stoner's instability constitutes a reconstruction of the Fermi surface of the unpolarized to the polarized gas due to interactions. However, this instability is quite naturally in competition with the reconstruction of the Fermi surface related to spin and charge density waves⁴¹⁻⁴³ (not addressed in this work) or Brillouin zone formation for Wigner crystallization. Despite the quite different interparticle interaction, hard or soft core potentials, the Stoner transition to a spin-polarized phase predicted within mean-field arguments seems to be quite generally preceded by transition to a crystalline phase for homogeneous systems with spin-independent interactions.

We acknowledge the CINECA award under the ISCRA initiative for the availability of high performance computing resources and the Fondation NanoSciences (Grenoble) for support. Part of the computations were performed using the Froggy platform of the CIMENT infrastructure, which is supported by the Rhône-Alpes region (grant CPER07-13 CIRA) and the project Equip@Meso (ANR-10-EQPX-29-01) of the ANR.

¹ F. Bloch, *Zeitschrift f. Physik* **57**, 545 (1929).
² E. P. Wigner, *Phys. Rev.* **46**, 1002 (1934).
³ E. P. Wigner, *Trans. Farad. Soc.* **34**, 678 (1938).
⁴ E.C. Stoner, *Proc. R. Soc. Lond. A* **165**, 372 (1938).
⁵ D. Ceperley, *Phys. Rev. B* **18**, 3126 (1978).
⁶ D. M. Ceperley and B. J. Alder, *Phys. Rev. Lett.* **45**, 566 (1980).
⁷ D. M. Ceperley and B. J. Alder, *Journal de Physique C* **7**, 295 (1980).
⁸ B.J. Alder, D.M. Ceperley, and E.L. Pollock, *Int. J. Quant. Chem.* **16**, 49 (1982).
⁹ G. Ortiz, M. Harris, and P. Ballone, *Phys. Rev. Lett.* **82**, 5317 (1999).
¹⁰ F. H. Zong, C. Lin, and D. M. Ceperley, *Phys. Rev. E* **66**,

036703 (2002).
¹¹ N. D. Drummond, Z. Radnai, J. R. Trail, M. D. Towler, and R. J. Needs, *Phys. Rev. B* **69**, 085116 (2004).
¹² D.P. Young, D. Hall, M.E. Torelli, Z. Fisk, J.L. Sarrao, J.D. Thompson, H.-R. Ott, S.B. Oseroff, R.G. Goodrich, and R. Zysler, *Nature (London)* **397**, 412 (1999).
¹³ S. Ichimaru, *Phys. Rev. Lett.* **84**, 1842 (2000).
¹⁴ G. Ortiz, M. Harris, and P. Ballone, *Phys. Rev. Lett.* **84**, 1843 (2000).
¹⁵ G.-B. Jo1, Y.-R. Lee, J.-H. Choi, C. A. Christensen, T. H. Kim, J. H. Thywissen, D. E. Pritchard, W. Ketterle, *Science* **325**, 1521 (2009).
¹⁶ G. Valtolina, F. Scazza, A. Amico, A. Burchianti, A. Recati, T. Enss, M. Inguscio, M. Zaccanti, and G. Roati,

- Nature Physics **13**, 704 (2017).
- ¹⁷ M. Taddei, M. Ruggeri, S. Moroni, and M. Holzmann, Phys. Rev. B **91**, 115106 (2015).
- ¹⁸ M. Ruggeri, S. Moroni, and M. Holzmann, Phys. Rev. Lett. **120**, 205302 (2018).
- ¹⁹ L.K. Wagner and D.M. Ceperley, Rep. Prog. Phys. **79**, 094501 (2016).
- ²⁰ G. Ortiz, D.M. Ceperley, and R.M. Martin, Phys. Rev. Lett. **71**, 2777 (1993).
- ²¹ C. Lin, F.-H. Zong, and D. M. Ceperley, Phys. Rev. E **64**, 016702 (2001).
- ²² S. Chiesa, D.M. Ceperley, R.M. Martin, and M. Holzmann, Phys. Rev. Lett. **97**, 076404 (2006).
- ²³ M. Holzmann, R.C. Clay III, M. A. Morales, N.M. Tubman, D. M. Ceperley, and C. Pierleoni, Phys. Rev. B **94**, 035126 (2016).
- ²⁴ N.D. Drummond, R.J. Needs, A. Sorouri, and W.M.C. Foulkes, Phys. Rev. B **78**, 125106 (2008).
- ²⁵ F. Rapisarda and G. Senatore, Aust. J. Phys. **49**, 161 (1996).
- ²⁶ D. Varsano, S. Moroni and G. Senatore, Europhys. Lett. **53**, 348 (2001).
- ²⁷ C. Attaccalite, S. Moroni, P. Gori-Giorgi, and G. B. Bachelet, Phys. Rev. Lett. **88**, 256601 (2002).
- ²⁸ N. D. Drummond and R. J. Needs Phys. Rev. Lett. **102**, 126402 (2009).
- ²⁹ G. F. Giuliani and G. Vignale, Quantum Theory of the Electron Liquid (Cambridge University Press, Cambridge, 2005).
- ³⁰ R.M. Martin, L. Reining, and D. M. Ceperley, Interacting Electrons, Cambridge University Press, Cambridge (2016).
- ³¹ P.P. Ewald, Ann. Phys. **64**, 253 (1921).
- ³² V. Natoli and D.M. Ceperley, J. Comput. Phys. **117**, 171 (1995).
- ³³ See Supplemental Material for details of the simulations, interpolations of the polarization energy, finite-size corrections, and tables with all QMC data and their zero-variance extrapolations.
- ³⁴ M. Holzmann, D.M. Ceperley, C. Pierleoni, and K. Esler, Phys. Rev. E **68**, 046707 (2003).
- ³⁵ M. Holzmann, B. Bernu, and D. M. Ceperley, J. Phys.: Conf. Ser. **321** 012020 (2011).
- ³⁶ M. Ruggeri, P. López Ríos, and A. Alavi, Phys. Rev. B **98**, 161105(R) (2018).
- ³⁷ G.G. Spink, R.J. Needs, and N.D. Drummond, Phys. Rev. B **88**, 085121 (2013).
- ³⁸ M. Nava, A. Motta, D. E. Galli, E. Vitali, and S. Moroni, Phys. Rev. B **85**, 184401 (2012).
- ³⁹ M. Holzmann, B. Bernu, and D.M. Ceperley, Phys. Rev. B **74**, 104510 (2006).
- ⁴⁰ T. Comparin, R. Bombin, M. Holzmann, F. Mazzanti, J. Boronat, and S. Giorgini, Phys. Rev. A **99**, 043609 (2019).
- ⁴¹ A. W. Overhauser, Phys. Rev. Lett. **4**, 462 (1960); Phys. Rev. **128**, 1437 (1962).
- ⁴² F. Delyon, B. Bernu, L. Baguet, and M. Holzmann, Phys. Rev. B **92**, 235124 (2015).
- ⁴³ D. Gontier, C. Hainzl, and M. Lewin, Phys. Rev. A **99**, 052501 (2019).

SUPPLEMENTAL MATERIAL

This supplemental materials contains (a) details of the DMC simulations, (b) a discussion of the interpolation for the polarization energy, (c) a test of the size extrapolation, and (d) tables with all the finite-size energies and variances for different wave functions, densities and polarizations, as well as their zero-variance extrapolations and finite-size corrections.

Details of the simulations

The calculations presented in the main text have been done for $N = 66$ electrons in twist averaged boundary conditions, using a regular grid of 1000 twists $\theta_\alpha = (m + 1/2)\pi/ML$ with $m = -M, -M + 1, \dots, M - 1$ and $M = 5$ ($\alpha = x, y, z$ and L is the linear extension of the cubic simulation cell). Care must be exerted when employing a regular grid of twists³⁶. Using VMC simulations with a SJ wave function, we have verified that the twist-averaged energy is converged within the accuracy of our calculations with respect to M , by comparison with a twist mesh with $M = 10$ and $\theta_\alpha = m\pi/ML$ with $m = -M, \dots, M - 1$. We further ruled out any significant bias in our regular-mesh results performing tests against unbiased averages over random twists uniformly sampled in the Brillouin zone, as well as against exact twist averaging^{22,23,36}; some of the results of exact twist averaging are shown in the section on the size extrapolation, see below. The wave functions are optimized by minimizing the twist-averaged energy. DMC energies are calculated with 1280 walkers and time step 15, 20, and 30 Ry⁻¹ for $r_s = 70, 100$, and 120, respectively. Population control bias and time step error are estimated to be of order of 10^{-7} Ry and 10^{-8} Ry, respectively, as illustrated in Fig. 5 for $r_s = 100$ at polarization $\zeta = 0$ with a BF2 trial wave function.

Interpolation of different functional forms for the polarization energy

All of our QMC calculations are done on a grid of few different polarizations, $\zeta = 0, 0.18, 0.42, 0.61, 0.79$, and 1, yielding a minimum of the energies at the unpolarized state. Since the polarization energies become less stiff at lower

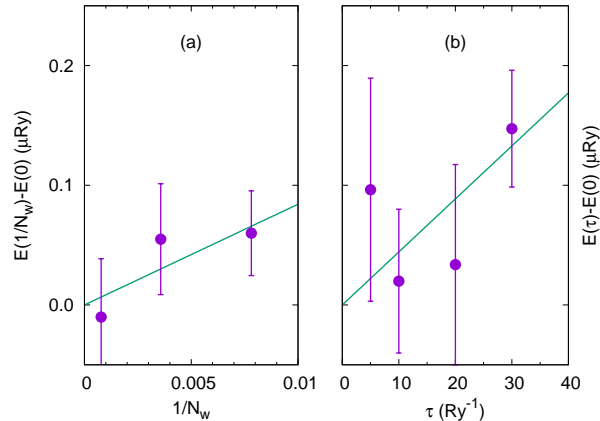


FIG. 5. Extrapolation of the DMC energy to (a) infinite number of walkers N_W and (b) zero time step τ , for $r_s = 100$ at polarization $\zeta = 0$ using a BF2 trial wave function. The bias for given τ or N_W is estimated as the corresponding value of the linear fit.

densities, the energy resolution needed to directly exclude a partially polarized ground state of small polarizations becomes rapidly unaffordable. The occurrence or absence of a partially polarized state can still be addressed considering possible functional forms of the polarization energy, $E_p(\zeta) \equiv E(\zeta) - E(0)$.

The simplest functional form assumes a polynomial dependence, $E(\zeta) = \alpha_0 + \sum_n \alpha_n \zeta^n$, containing only even powers of ζ . Given the limited number of data points we can fit, and their statistical errors, we can only pin down the value of a restricted number of parameters. In order to gain some confidence on the robustness of the results, we also fit a completely different functional form, suggested by the presence of a Slater determinant of plane waves in the wave function (either SJ or BFk), which assumes a polynomial dependence of the exchange-correlation energy, $E_{XC}(\zeta) \equiv E(\zeta) - E_{id}(\zeta) = \beta_0 + \sum_n \beta_n \zeta^n$, where $E_{id}(\zeta) = \left(\frac{9\pi}{4}\right)^{2/3} \frac{3}{10r_s^2} [(1 + \zeta)^{5/3} + (1 - \zeta)^{5/3}]$ is the ideal gas energy. The best fits obtained using both functional forms with various combinations of powers of ζ up to 6 are illustrated in Fig. 6 for $r_s = 100$ and Fig. 7 for $r_s = 120$. For $r_s = 100$ all fits give the lowest energy for $\zeta = 0$. The second order term in the expansion of $E(\zeta)$, related to the inverse spin susceptibility, is larger than the statistical uncertainty in all cases but the top right panel, which however has a poor χ^2 . The second smallest term of second order is found in the bottom middle panel, again with a rather large χ^2 . The inclusion of more powers of ζ (left panels) begins to overfit the data, because it does not decrease significantly the χ^2 . Interestingly, however, it does support the fits with fewer parameters which yield smaller χ^2 and larger second order terms. For $r_s = 120$, $E(\zeta)$ has a minimum for a finite polarization in the top right panel (barely visible in the figure) and in the bottom middle panels (ten times shallower). However the top middle and bottom right panels both give the energy minimum at $\zeta = 0$, with a_2 positive and larger in modulus, and smaller χ^2 . Again, the inclusion of more powers of ζ in the left panels results in a little overfit, supporting however the fits with fewer parameters which yield smaller χ^2 and positive second order terms. We conclude that the fluid phase is definitely paramagnetic at $r_s = 100$. For $r_s = 120$ it is most likely paramagnetic, possibly on the verge of spin polarization; however at this density the ground state is already the Wigner crystal. It turns out that in all cases $E(\zeta)$, beyond the term quadratic in ζ , is well represented by only one dominant higher-order contribution, with a positive coefficient. In this situation, the existence of a partially polarized phase is linked to the sign of a_2 , and its confidence levels can be directly inferred from the values of a_2 and their uncertainties, shown in Figs. 6 and 7.

We now address the dependence on the choice of the QMC data set. Above, we have considered DMC zero-variance extrapolations without the SJ results. Using the DMC data set which includes the SJ results, we find generally higher values of a_2 , albeit with a somewhat larger χ^2 . This makes a stronger case for the paramagnetic fluid. An example for the fit of $E(\zeta)$ at $r_s = 100$ is given in Table I. The VMC data sets, either with or without the SJ results, have rather large statistical uncertainties, so that $E(\zeta)$ is already well fitted using only two powers of ζ . For both $r_s = 100$ and 120 the choice of powers 0 and 6 gives the lowest χ^2 , and of course $a_2 = 0$. The inclusion of a quadratic term does not change the reduced χ^2 and leaves a_2 largely undetermined. For $r_s = 100$, we report the results in Table I. The VMC results are consistent with a paramagnetic ground state of the fluid phase.

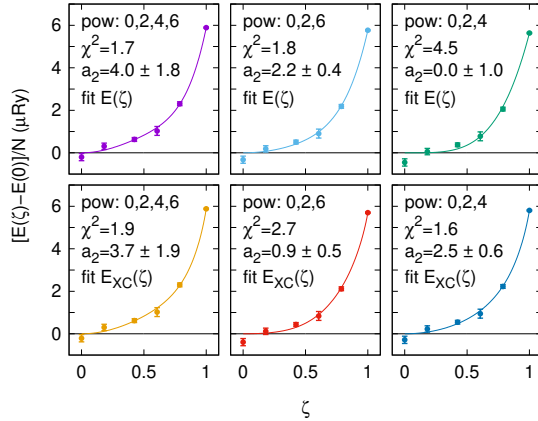


FIG. 6. The polarization energy per particle for $r_s = 100$ obtained from the best fit of various functional forms: upper panels, fit of $E(\zeta)$; lower panels, fit of $E_{XC}(\zeta)$; left panels, powers 0, 2, 4, 6 of ζ (see text); middle panels, powers 0, 2, 6; right panels, powers 0, 2, 4. The reference value $E(0)$ is the energy at zero polarization resulting from the fit. The data used are DMC zero-variance extrapolations w/o SJ. In each panel, we list the powers of ζ employed in the fit, the reduced χ^2 , and the resulting coefficient a_2 of the second order term in $E(\zeta)$.

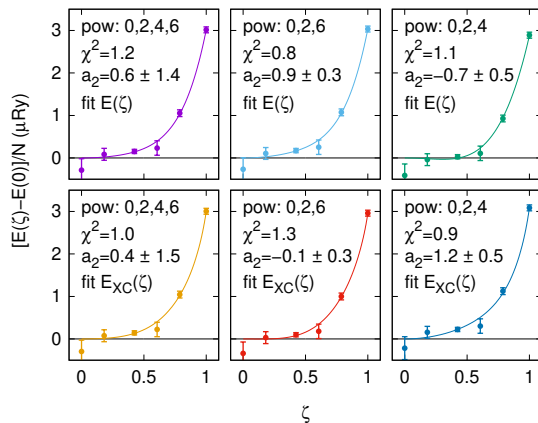


FIG. 7. Same as Fig. 6 for $r_s = 120$.

Size Extrapolation: Numerical study with SJ and BF VMC

Size extrapolations to the thermodynamic limit presents one of the major sources of systematic bias of our QMC calculations. By construction, the functional form of backflow wave functions is size consistent due to the extensivity of the logarithm of the trial wave function, which has been shown explicitly for Slater Jastrow wave functions with and without backflow^{22–24} as well as with iterated backflow wave functions¹⁷. However, explicit numerical extrapolation to the thermodynamic limit is computational expensive, e.g. as the quality of the optimization within VMC as well as time step and population bias in DMC must be controlled carefully to avoid loss of quality in the description for increasing system sizes biasing the extrapolation. Above and in the main paper, we have used thermodynamic limit extrapolations based on finite size corrections obtained from correlation functions²³ which have been shown to reach accuracies comparable to explicit numerical extrapolations.

Typically, reaching the asymptotic region where finite size corrections can be successfully applied is easier in the

data set	powers of ζ	χ^2	a_2
VMC full	0,6	0.2	0
	0,2,6	0.2	0.7 ± 0.6
VMC w/o SJ	0,6	0.1	0
	0,2,6	0.1	0.4 ± 0.5
DMC full	0,2,4	3.8	0.6 ± 0.9
	0,2,6	2.4	2.5 ± 0.5
	0,2,4,6	3.5	3.4 ± 2.6
DMC w/o SJ	0,2,4	4.5	0.0 ± 1.0
	0,2,6	1.8	2.2 ± 0.4
	0,2,4,6	1.7	4.0 ± 1.8

TABLE I. Reduced χ^2 and coefficient a_2 of the second order term in a polynomial fit of $E(\zeta)$ for $r_s = 100$, using various powers of ζ and various data sets.

low density region where the potential energy dominates. Quasirandom contributions, posing difficulties in the high density region $r_s \lesssim 1$ addressed in Refs. 36 and 37, are expected to be less relevant there. Ref. 10 has already shown that twist average, together with the leading order $1/N$ corrections, provides accurate extrapolations to the thermodynamic limit in the region $50 \leq r_s \leq 100$. In the following, we provide further tests using Slater Jastrow wave functions with the analytical Jastrow potential of Ref. 34 to verify our finite-size extrapolations. We assume that size effects are to a large extent transferable to the more correlated wave functions, e.g. two-particle size corrections from backflow as discussed in Ref. 23 are suppressed by $1/r_s$ and negligible in the considered large r_s region. The SJ VMC study thus provides an independent test of the accuracy of our extrapolations. Transferability has been checked in a few relevant cases using the analytical backflow wave function of Ref. 34.

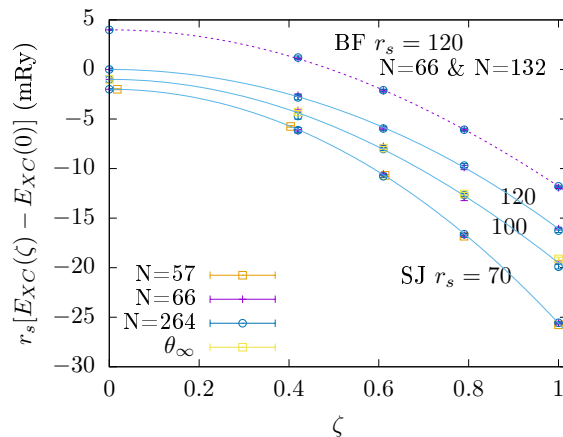


FIG. 8. Exchange-correlation part of twist averaged polarization energies, $E_{XC}(\zeta) - E_{XC}(0)$, for SJ VMC wave functions with analytical Jastrow potentials for $N = 66$ and $N = 264$ electrons at the three different densities together with the corresponding polynomial approximation of degree 2 and 4, yielding values of χ^2 per degree of freedom of 1.0 ($r_s = 70$), 0.5 ($r_s = 100$), and 0.8 ($r_s = 120$). Curves for $r_s = 100$ and $r_s = 70$ are shifted by a negative constant offset. For $r_s = 70$ we plot also the twist averaged energies for $N = 57$ electrons which would correspond to a closed shell of the fully polarized system at the Gamma point (zero twist). With a positive constant offset we plot the polarization energies of $N = 66$ compared to $N = 132$ electrons using analytical backflow wave functions at $r_s = 120$. The polynomial fit of degree 2 and 4, shown as dashed line, has a $\chi^2 = 0.3$ per degree of freedom. For $N = 66$ at $r_s = 100$ we also show, in yellow squares, the results obtained with exact twist averaging²².

Leading order two-body corrections to the total energy are due to collective plasmon excitations^{22,35}. They only depend on the total density and are not sensitive to spin polarization. Therefore, the polarization energy is expected to approach the thermodynamic limit more rapidly than the total energy. Figure 8 shows the exchange-correlation part of the polarization energies for our three densities from calculations with $N = 66$ and $N = 264$: systematic finite size bias is not visible within the accuracy.

In order to check the relevance of quasirandom fluctuations³⁶ we have performed calculations for $N = 57$ having a

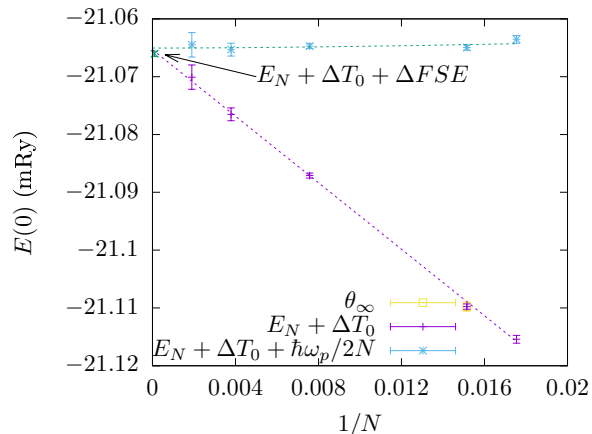


FIG. 9. Numerical extrapolation of twist-averaged energies of SJ VMC wave functions with analytical Jastrow potential for $N = 57$, $N = 66$, 132, and 264 electrons at $r_s = 70$ and zero polarization corrected by the ideal gas kinetic energy corrections, $E_N + \Delta T_0$, together with the energy values including the analytical leading order $1/N$ (Plasmon) correction, $E_N + \Delta T_0 + \hbar\omega_p/2N$ with $\hbar\omega_p/2 = \sqrt{3}/r_s^3$ Ry. The lines are based on fitting linear and $N^{-5/3}$ corrections for $E_N + \Delta T_0$ and only $N^{-5/3}$ corrections for $E_N + \Delta T_0 + \hbar\omega_p/2N$. At the origin we show the value obtained from the value of $N = 66$ corrected by ΔT_0 and 2-body finite size corrections ΔFSE obtained from interpolating the structure factor as given in the tables. The result for $N = 66$ shown by the yellow square labeled with θ_∞ has been obtained with exact twist averaging²².

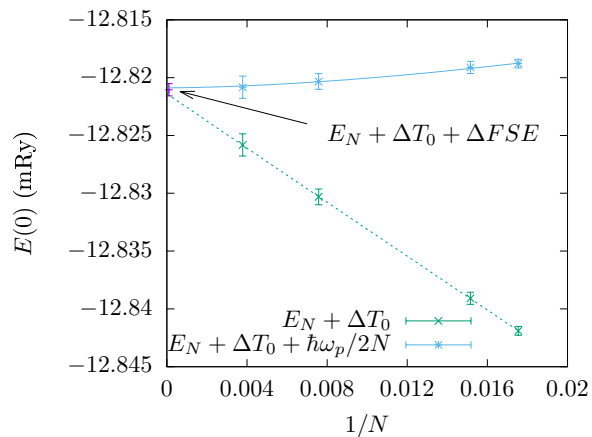


FIG. 10. Numerical extrapolation of twist-averaged energies of BF VMC wave functions with analytical Jastrow and backflow potential for $N = 57$, $N = 66$, 132, and 264 electrons at $r_s = 120$ and zero polarization corrected by the ideal gas kinetic energy corrections, $E_N + \Delta T_0$, together with the energy values including the analytical leading order $1/N$ (Plasmon) correction, $E_N + \Delta T_0 + \hbar\omega_p/2N$ with $\hbar\omega_p/2 = \sqrt{3}/r_s^3$ Ry. The lines are based on fitting linear and $N^{-5/3}$ corrections for $E_N + \Delta T_0$ and only $N^{-5/3}$ corrections for $E_N + \Delta T_0 + \hbar\omega_p/2N$. At the origin we show the value obtained from the value of $N = 66$ corrected by ΔT_0 and 2-body finite size corrections ΔFSE obtained from interpolating the structure factor as given in the tables.

closed shell for the fully polarized state, in contrast to $N = 66$ with closed shell at the Gamma point for the unpolarized state. From Fig. 8, we do not see any systematic bias within our uncertainty. Furthermore, we have checked the energy differences between the fully polarized and the unpolarized state at $r_s = 70$, yielding $E(\zeta = 1) - E(\zeta = 0) = 42.5(7)\mu\text{Ry}$ for $N = 66$, compared to $43.7(6)\mu\text{Ry}$ for $N = 57$, $41.4(9)\mu\text{Ry}$ for $N = 132$, and $= 41.8(15)\mu\text{Ry}$ for $N = 264$, all compatible within the error. Note that using canonical twist average, for $N = 57$ we are forced to consider slightly different polarizations than for $N = 66$ or 264, apart from the case of $\zeta = 1$. For $N = 57$, the value of $E(\zeta = 0)$ is estimated combining the calculated energy at $\zeta = 1/57$, the polynomial fit of the exchange correlation energy, and the ideal gas polarization energy.

We have also compared the polarization energy at $r_s = 120$ between systems with $N = 66$ and $N = 132$ electrons using analytical BF wave function³⁴ within VMC (Figure 8), yielding again no visible bias.

In Figure 9 we illustrate the size effects of the total energy at zero polarization at $r_s = 70$. Our finite size corrected

energies are generally within $1 \mu\text{Ry}$ of the numerical extrapolations. We take this value as an estimate of the systematic bias in the extrapolation to the thermodynamic limit. As another example, the numerical extrapolation of the VMC data with analytical backflow wave functions³⁴ with $N = 57, 66, 132,$ and 264 electrons at $r_s = 120$, shown in Fig. 10, agrees with the finite size corrected $N = 66$ data within the uncertainty. The numerical extrapolations of Figs. 9 and 10 are not sensitive to the precise power law assumed for the next-to-leading-order term. In the figures, we show the extrapolation based on a $N^{-5/3}$ behavior, as resulting from a regular expansion of the structure factor at the origin.

In the result for the Wigner crystallization density, $r_s = 113(2)$, the uncertainty includes both the statistical error on the Monte Carlo data and our estimate of the systematic bias in the size corrections.

Tables of QMC results

Tables II, III, and IV list all the finite-size energies and variances for different wave functions, densities and polarizations as specified in the main text, as well as zero-variance extrapolations and finite-size corrections.

ζ	Ψ	σ^2/σ_0^2	VMC	DMC	ΔT_0	ΔFSE
0.00	SJ	1.00000(326)	-21.17385(39)	-21.31364(28)	-0.00106	0.04373
	BF0	0.32706(91)	-21.31461(21)	-21.35302(12)	-0.00106	0.04079
	BF1	0.15819(51)	-21.34883(12)	-21.36427(07)	-0.00106	0.04097
	BF2	0.07838(25)	-21.36009(08)	-21.36794(08)	-0.00106	0.04117
	BF3	0.07079(28)	-21.36121(08)	-21.36841(03)	-0.00106	0.04180
	BF4	–	–	–	–	–
	ext full		-21.37267(160)	-21.37238(56)		
	ext w/o SJ		-21.36843(48)	-21.37090(26)		
0.42	SJ	0.96797(304)	-21.18668(40)	-21.31704(29)	-0.00053	0.04373
	BF0	0.30780(89)	-21.31742(19)	-21.35256(09)	-0.00053	0.04079
	BF1	0.13848(48)	-21.34880(12)	-21.36240(06)	-0.00053	0.04097
	BF2	0.08538(28)	-21.35649(09)	-21.36481(08)	-0.00053	0.04117
	BF3	0.07069(30)	-21.35860(08)	-21.36555(04)	-0.00053	0.04180
	BF4	–	–	–	–	–
	ext full		-21.37013(102)	-21.36941(38)		
	ext w/o SJ		-21.36710(32)	-21.36832(19)		
0.61	SJ	0.91064(303)	-21.19929(46)	-21.32103(23)	-0.00066	0.04373
	BF0	0.28858(86)	-21.32023(18)	-21.35184(07)	-0.00066	0.04079
	BF1	0.13152(42)	-21.34817(10)	-21.36046(06)	-0.00066	0.04097
	BF2	0.08425(28)	-21.35481(09)	-21.36249(04)	-0.00066	0.04117
	BF3	0.06870(56)	-21.35706(09)	-21.36316(03)	-0.00066	0.04180
	BF4	–	–	–	–	–
	ext full		-21.36794(97)	-21.36678(32)		
	ext w/o SJ		-21.36515(49)	-21.36563(13)		
0.79	SJ	0.81174(275)	-21.21608(37)	-21.32436(25)	-0.00074	0.04373
	BF0	0.26009(70)	-21.32214(17)	-21.34939(14)	-0.00074	0.04079
	BF1	0.12528(34)	-21.34535(09)	-21.35628(06)	-0.00074	0.04097
	BF2	0.08368(27)	-21.35111(07)	-21.35773(05)	-0.00074	0.04117
	BF3	0.06924(48)	-21.35314(07)	-21.35856(03)	-0.00074	0.04180
	BF4	–	–	–	–	–
	ext full		-21.36358(80)	-21.36170(40)		
	ext w/o SJ		-21.36116(44)	-21.36097(96)		
1.00	SJ	0.63694(203)	-21.23829(34)	-21.32189(21)	-0.00066	0.04373
	BF0	0.21696(58)	-21.31933(16)	-21.34051(07)	-0.00066	0.04079
	BF1	0.10935(31)	-21.33719(09)	-21.34574(04)	-0.00066	0.04097
	BF2	0.07083(24)	-21.34198(08)	-21.34700(05)	-0.00066	0.04117
	BF3	0.05861(16)	-21.34384(07)	-21.34774(05)	-0.00066	0.04180
	BF4	–	–	–	–	–
	ext full		-21.35177(67)	-21.35030(40)		
	ext w/o SJ		-21.35006(112)	-21.34945(77)		

TABLE II. Energy per particle (in mRy) at various spin polarizations ζ for $r_s = 70$ from VMC and DMC simulations of 66 electrons in twist-averaged boundary conditions using different wave functions, SJ and BF k ; variance of the local energy relative to that of the SJ wave function at $\zeta = 0$, σ^2/σ_0^2 ; zero-variance extrapolation of the VMC and DMC energies with or without the SJ result (“ext full” and “ext w/o SJ”, obtained using gnuplot and taking into account the standard deviations of both energy and variance); finite size errors for the discretization of k -space through the non-interacting shell effect, ΔT_0 , Eq.(22) of Ref. 23, and through integrals involving the static structure factor, ΔFSE , Eq.(30), (35), and (38) of Ref. 23. In the calculation of ΔFSE we use the RPA two-body pseudopotential and the analytic backflow; we also average over the polarizations because there is not enough statistical precision to detect a polarization dependence.

ζ	Ψ	σ^2/σ_0^2	VMC	DMC	ΔT_0	ΔFSE
0.00	SJ	1.00000(232)	-15.25228(13)	-15.35243(28)	-0.00052	0.02543
	BF0	0.34206(80)	-15.34443(13)	-15.37588(09)	-0.00052	0.02382
	BF1	0.15445(43)	-15.37101(08)	-15.38345(07)	-0.00052	0.02413
	BF2	0.09342(23)	-15.37899(06)	-15.38588(03)	-0.00052	0.02414
	BF3	0.07226(17)	-15.38112(05)	-15.38661(03)	-0.00052	0.02441
	BF4	0.06484(17)	-15.38189(04)	-15.38683(04)	-0.00052	0.02468
	ext full		-15.39050(57)	-15.38953(13)		
	ext w/o SJ		-15.38886(59)	-15.38914(17)		
0.18	SJ	0.98798(413)	-15.25354(34)	-15.35302(08)	-0.00039	0.02543
	BF0	0.33780(130)	-15.34508(18)	-15.37524(02)	-0.00039	0.02382
	BF1	0.15244(46)	-15.37101(11)	-15.38289(02)	-0.00039	0.02413
	BF2	0.09258(33)	-15.37890(08)	-15.38536(02)	-0.00039	0.02414
	BF3	0.07234(31)	-15.38086(07)	-15.38604(01)	-0.00039	0.02441
	BF4	0.06409(27)	-15.38161(06)	-15.38636(02)	-0.00039	0.02468
	ext full		-15.39001(63)	-15.38910(13)		
	ext w/o SJ		-15.38847(81)	-15.38876(15)		
0.42	SJ	0.91178(131)	-15.26052(11)	-15.35652(30)	-0.00026	0.02543
	BF0	0.32012(77)	-15.34784(12)	-15.37672(08)	-0.00026	0.02382
	BF1	0.14920(24)	-15.37188(06)	-15.38343(06)	-0.00026	0.02413
	BF2	0.09047(25)	-15.37929(06)	-15.38558(03)	-0.00026	0.02414
	BF3	-	-	-	-	-
	BF4	0.06415(18)	-15.38196(05)	-15.38645(03)	-0.00026	0.02468
	ext full		-15.39015(69)	-15.38899(16)		
	ext w/o SJ		-15.38876(64)	-15.38857(09)		
0.61	SJ	0.89692(241)	-15.26984(24)	-15.35928(33)	-0.00032	0.02543
	BF0	0.30266(85)	-15.35090(12)	-15.37749(10)	-0.00032	0.02382
	BF1	0.14164(36)	-15.37289(07)	-15.38338(06)	-0.00032	0.02413
	BF2	0.08791(24)	-15.37962(05)	-15.38536(04)	-0.00032	0.02414
	BF3	0.07001(65)	-15.38172(15)	-15.38582(03)	-0.00032	0.02441
	BF4	0.06261(18)	-15.38209(04)	-15.38611(03)	-0.00032	0.02468
	ext full		-15.39009(58)	-15.38846(13)		
	ext w/o SJ		-15.38857(62)	-15.38811(21)		
0.79	SJ	0.81249(244)	-15.28176(22)	-15.36306(23)	-0.00036	0.02543
	BF0	0.27848(73)	-15.35429(12)	-15.37792(09)	-0.00036	0.02382
	BF1	0.13232(37)	-15.37342(06)	-15.38282(03)	-0.00036	0.02413
	BF2	0.08441(22)	-15.37923(05)	-15.38435(02)	-0.00036	0.02414
	BF3	0.06808(16)	-15.38081(05)	-15.38484(02)	-0.00036	0.02441
	BF4	0.06179(20)	-15.38135(04)	-15.38499(02)	-0.00036	0.02468
	ext full		-15.38877(44)	-15.38706(10)		
	ext w/o SJ		-15.38758(52)	-15.38679(09)		
1.00	SJ	0.67302(100)	-15.29788(10)	-15.36486(22)	-0.00032	0.02543
	BF0	0.24224(67)	-15.35647(10)	-15.37570(08)	-0.00032	0.02382
	BF1	0.11261(29)	-15.37226(07)	-15.37986(05)	-0.00032	0.02413
	BF2	0.07619(22)	-15.37678(05)	-15.38098(04)	-0.00032	0.02414
	BF3	0.06177(20)	-15.37821(03)	-15.38141(02)	-0.00032	0.02441
	BF4	0.05502(14)	-15.37866(04)	-15.38163(03)	-0.00032	0.02468
	ext full		-15.38499(35)	-15.38347(06)		
	ext w/o SJ		-15.38435(81)	-15.38325(03)		

TABLE III. Same as Table II for $r_s = 100$.

ζ	Ψ	σ^2/σ_0^2	VMC	DMC	ΔT_0	ΔFSE
0.00	SJ	1.0000(30)	-12.87447(19)	-12.95868(20)	-0.00036	0.01930
	BF0	0.3557(10)	-12.94860(12)	-12.97655(07)	-0.00036	0.01803
	BF1	0.1728(04)	-12.97104(05)	-12.98269(08)	-0.00036	0.01883
	BF2	0.1026(03)	-12.97875(04)	-12.98476(03)	-0.00036	0.01876
	BF3	0.0804(02)	-12.98078(04)	-12.98557(03)	-0.00036	0.01886
	BF4	0.0716(02)	-12.98137(04)	-12.98572(02)	-0.00036	0.01893
	ext full		-12.98943(65)	-12.98819(12)		
	ext w/o SJ		-12.98782(59)	-12.98786(27)		
0.18	SJ	0.97644(451)	-12.87615(25)	-12.96060(34)	-0.00027	0.01930
	BF0	0.35345(134)	-12.94900(13)	-12.97625(32)	-0.00027	0.01803
	BF1	0.17149(62)	-12.97128(09)	-12.98218(25)	-0.00027	0.01883
	BF2	0.10206(36)	-12.97862(07)	-12.98456(51)	-0.00027	0.01876
	BF3	0.07986(30)	-12.98060(06)	-12.98509(34)	-0.00027	0.01886
	BF4	0.07087(28)	-12.98124(06)	-12.98538(23)	-0.00027	0.01893
	ext full		-12.98900(68)	-12.98786(14)		
	ext w/o SJ		-12.98720(43)	-12.98758(12)		
0.42	SJ	0.96287(299)	-12.88101(24)	-12.96112(18)	-0.00018	0.01930
	BF0	0.33762(89)	-12.95121(10)	-12.97750(06)	-0.00018	0.01803
	BF1	0.16520(45)	-12.97204(06)	-12.98279(03)	-0.00018	0.01883
	BF2	0.09907(26)	-12.97913(04)	-12.98477(03)	-0.00018	0.01876
	BF3	0.07704(19)	-12.98108(04)	-12.98537(03)	-0.00018	0.01886
	BF4	0.06876(19)	-12.98179(03)	-12.98564(03)	-0.00018	0.01893
	ext full		-12.98943(57)	-12.98780(07)		
	ext w/o SJ		-12.98777(37)	-12.98760(05)		
0.61	SJ	0.91729(294)	-12.88814(19)	-12.96447(21)	-0.00022	0.01930
	BF0	0.32041(99)	-12.95415(10)	-12.97834(06)	-0.00022	0.01803
	BF1	0.15444(40)	-12.97320(05)	-12.98313(04)	-0.00022	0.01883
	BF2	0.09523(23)	-12.97963(05)	-12.98488(03)	-0.00022	0.01876
	BF3	0.07506(18)	-12.98150(04)	-12.98546(02)	-0.00022	0.01886
	BF4	0.06584(20)	-12.98211(04)	-12.98562(02)	-0.00022	0.01893
	ext full		-12.98939(48)	-12.98768(09)		
	ext w/o SJ		-12.98822(63)	-12.98748(17)		
0.79	SJ	0.83963(256)	-12.89765(20)	-12.96749(13)	-0.00025	0.01930
	BF0	0.29635(74)	-12.95744(10)	-12.97902(11)	-0.00025	0.01803
	BF1	0.14659(39)	-12.97407(07)	-12.98321(03)	-0.00025	0.01883
	BF2	0.09018(23)	-12.97979(04)	-12.98461(03)	-0.00025	0.01876
	BF3	0.07189(18)	-12.98147(03)	-12.98508(02)	-0.00025	0.01886
	BF4	0.06351(18)	-12.98203(04)	-12.98522(02)	-0.00025	0.01893
	ext full		-12.98867(39)	-12.98689(11)		
	ext w/o SJ		-12.98751(44)	-12.98663(08)		
1.00	SJ	0.71979(221)	-12.91080(17)	-12.96998(18)	-0.00022	0.01930
	BF0	0.26296(59)	-12.96006(09)	-12.97809(05)	-0.00022	0.01803
	BF1	0.12702(33)	-12.97426(05)	-12.98178(04)	-0.00022	0.01883
	BF2	0.08318(39)	-12.97891(05)	-12.98289(02)	-0.00022	0.01876
	BF3	0.06682(18)	-12.98021(04)	-12.98324(02)	-0.00022	0.01886
	BF4	0.06109(35)	-12.98067(03)	-12.98338(02)	-0.00022	0.01893
	ext full		-12.98687(25)	-12.98516(12)		
	ext w/o SJ		-12.98632(53)	-12.98470(07)		

TABLE IV. Same as Table II for $r_s = 120$.